

## Supporting Information

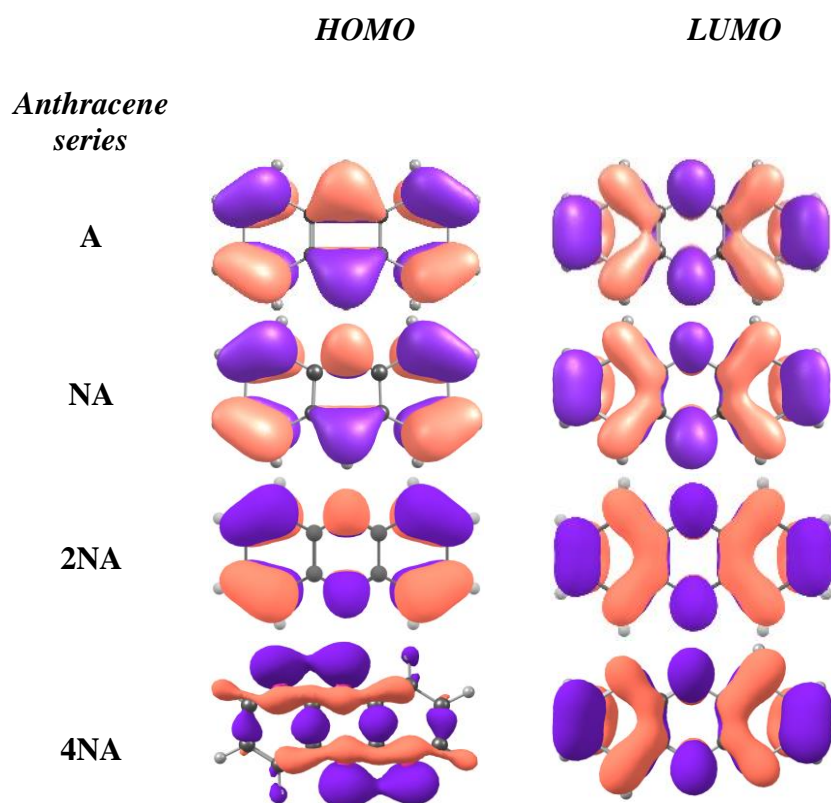
### Tuning of molecular electrostatic potential enables efficient charge transport in crystalline azaacenes: a computational study

Andrey Yu. Sosorev<sup>1,2\*</sup>, Dmitry I. Dominskiy<sup>3</sup>, Ivan Yu. Chernyshov<sup>4</sup>, Roman G. Efremov<sup>1</sup>

1. *Shemyakin-Ovchinnikov Institute of bioorganic chemistry of the Russian Academy of Sciences, Ulitsa Miklukho-Maklaya, 16/10, Moscow, GSP-7, 117997, Russia*
2. *Institute of Spectroscopy of the Russian Academy of Sciences, Fizicheskaya Str., 5, Troitsk, Moscow 108840, Russia*
3. *Faculty of Physics and International Laser Center, Lomonosov Moscow State University, Leninskie Gory 1/62, Moscow 119991, Russia*
4. *TheoMAT Group, ChemBio cluster, ITMO University, Lomonosova 9, St. Petersburg 191002, Russia*

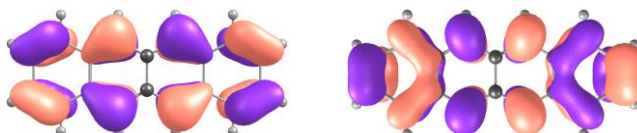
\*e-mail: sosorev@physics.msu.ru

#### S1. Individual molecules: details

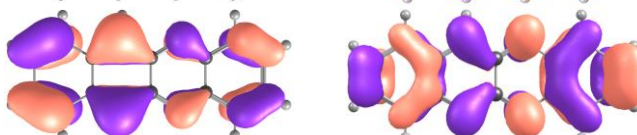


*Tetracene*  
*series*

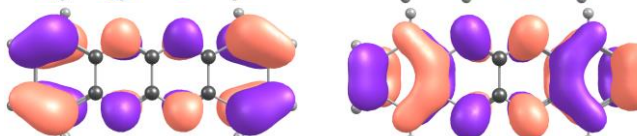
**T**



**2NT**

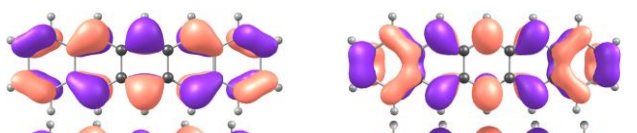


**4NT**

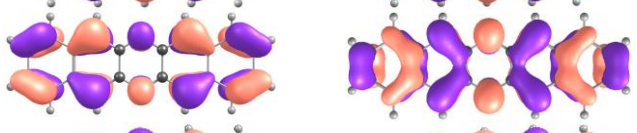


*Pentacene*  
*series*

**P**



**2NP**



**4NP**

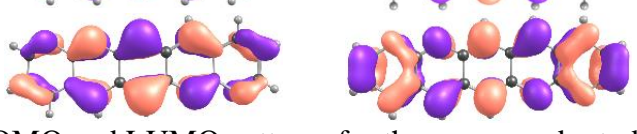
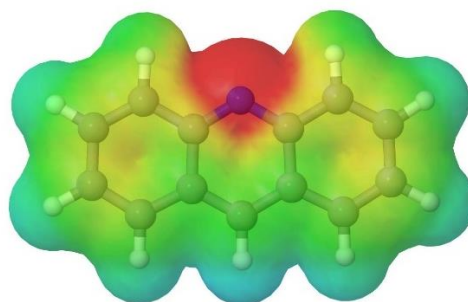
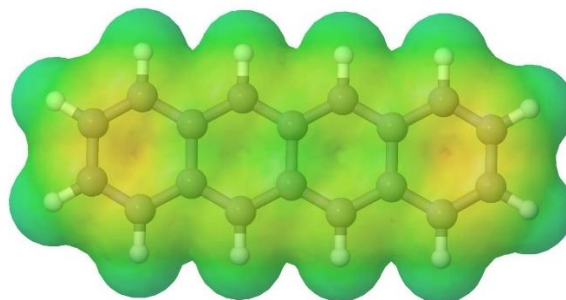


Figure S1. HOMO and LUMO patterns for the compounds studied.

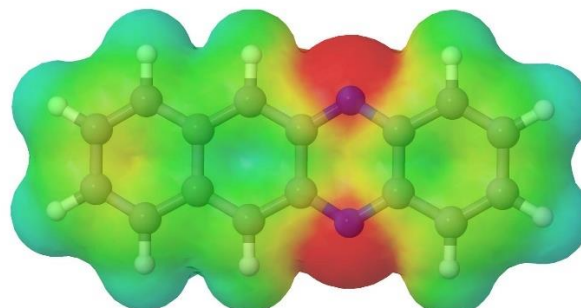
**NA**



**T**



**2NT**



**4NT**

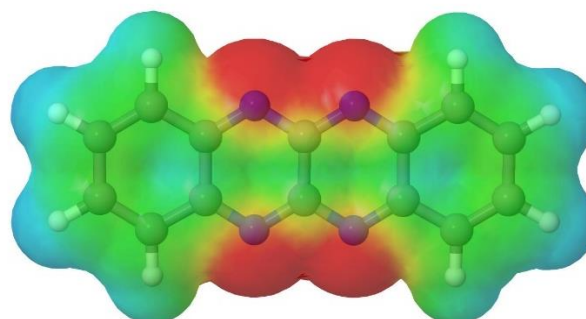


Figure S2. Molecular electrostatic potentials (ESPs) for the selected compounds studied.

S2. Crystals: details  
CCDC codes

Table S1. CCDC entry codes for the crystals studied.

<i>compound</i>	<i>Abbreviation</i>	<i>CCDC code</i>
anthracene	A	1103074
phenazine	2NA	1232385
dipyrido[2,3-b:2',3'-e]pyrazine	4NA	720329
tetracene	T	114446
benzo[b]phenazine	2NT	696053
quinoxalino[2,3-b]quinoxaline	4NT	297949
pentacene	P	114447
dibenzo[b,i]phenazine	2NP	N/A*
benzo[1,2-b:4,5-b']bis[1,8]naphthyridine	4NP	1866946

\*obtained from Prof. Q. Miao.

Anthracene and derivatives

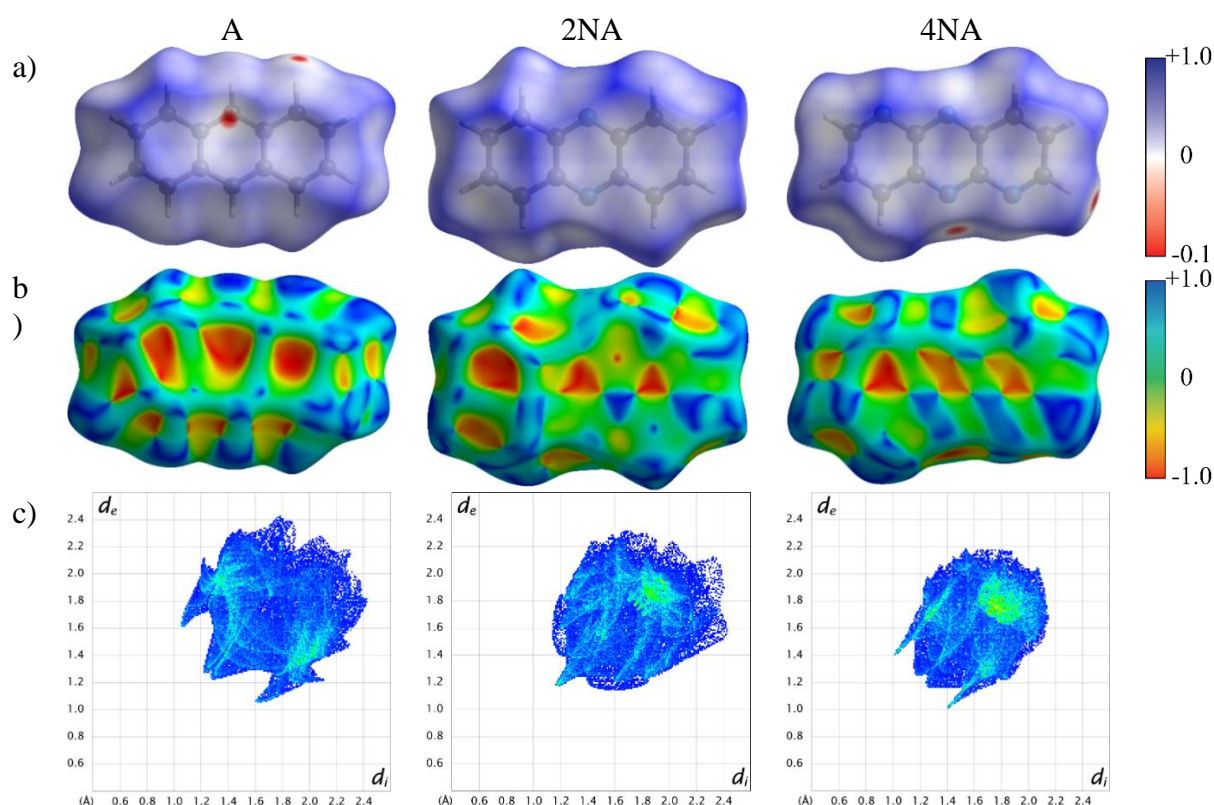


Figure S3. Hirshfeld surfaces of **A**, **2NA** and **4NA** mapped with normalized contact distance (a) and shape index (b). Red spots in (a) indicate intermolecular contacts closer than the sum of the van-der-Waals radii (close contacts), blue spots are referred to longer contacts, and contacts around the sum of van-der-Waals radii (moderate contacts) are white. 2D fingerprint plots (c) with  $d_i$  (distance from the atom inside the Hirshfeld surface) and  $d_e$  (distance from the atom outside the Hirshfeld surface) ranging from 0.5 to 2.9 Å. For any given  $d_i$  and  $d_e$  pairs, the change in color shows the raise in occurrence: white color for no occurrence, then blue green and red for the most frequent occurrence.

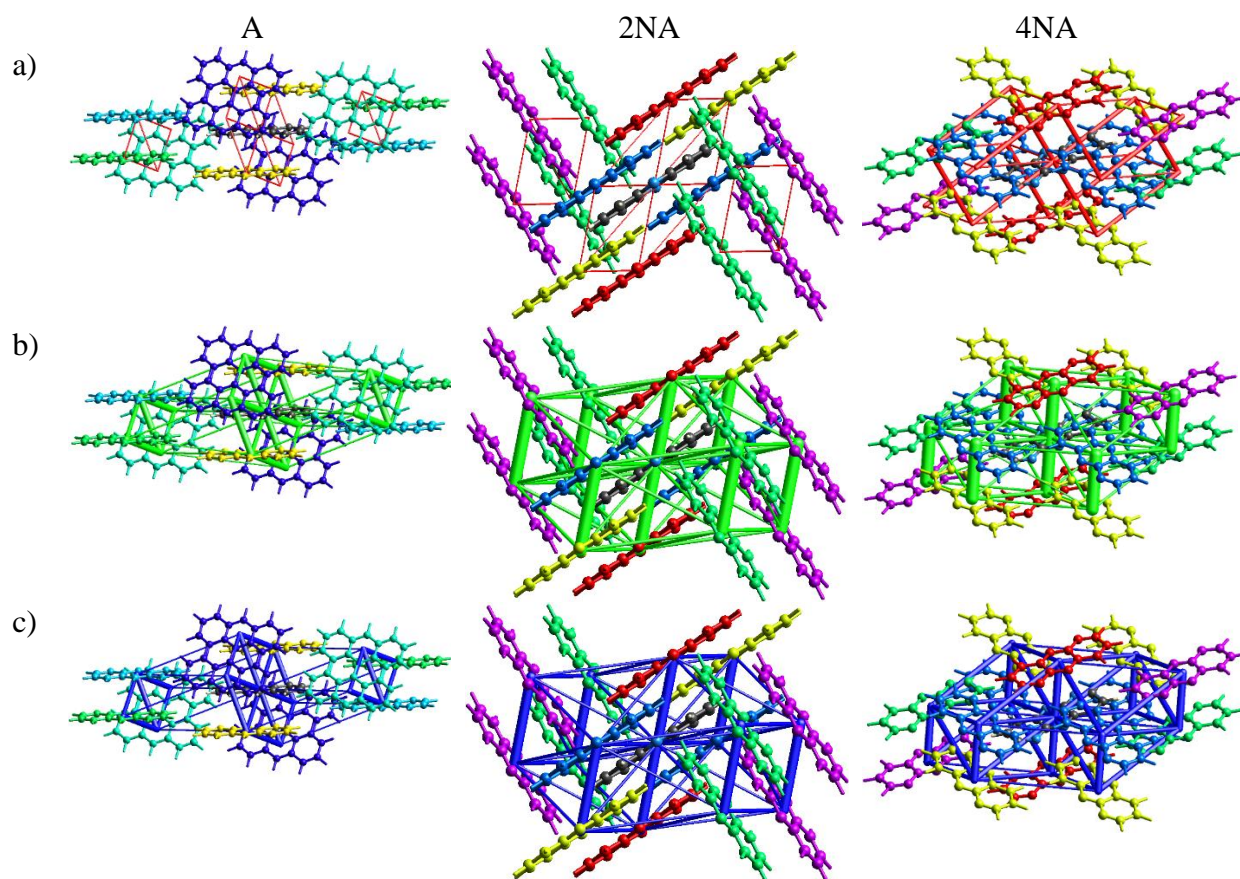


Figure S4. Graphical representation of intermolecular interactions (the Coulomb interaction energy in red on the panel a, the dispersion energy in green on the panel b, and the total interaction energy in blue on the panel c) in **A** (the first column), **2NA** (the second column) and **4NA** (the third column) crystals. The cylinders link molecular centroids, and their thickness is proportional to the magnitude of the energy; for clarity, pairwise energies with magnitudes less than 5 kJ mol<sup>-1</sup> are omitted.

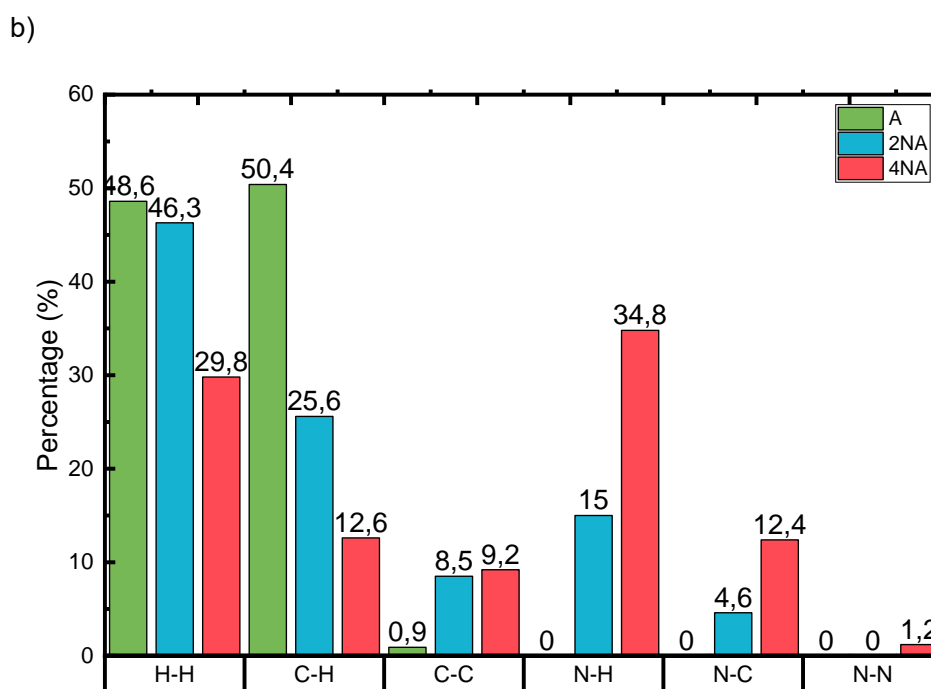


Figure S5. Distribution of reciprocal intermolecular contacts for **A**, **2NA** and **4NA** arranged by atom types.

Tetracene and derivatives

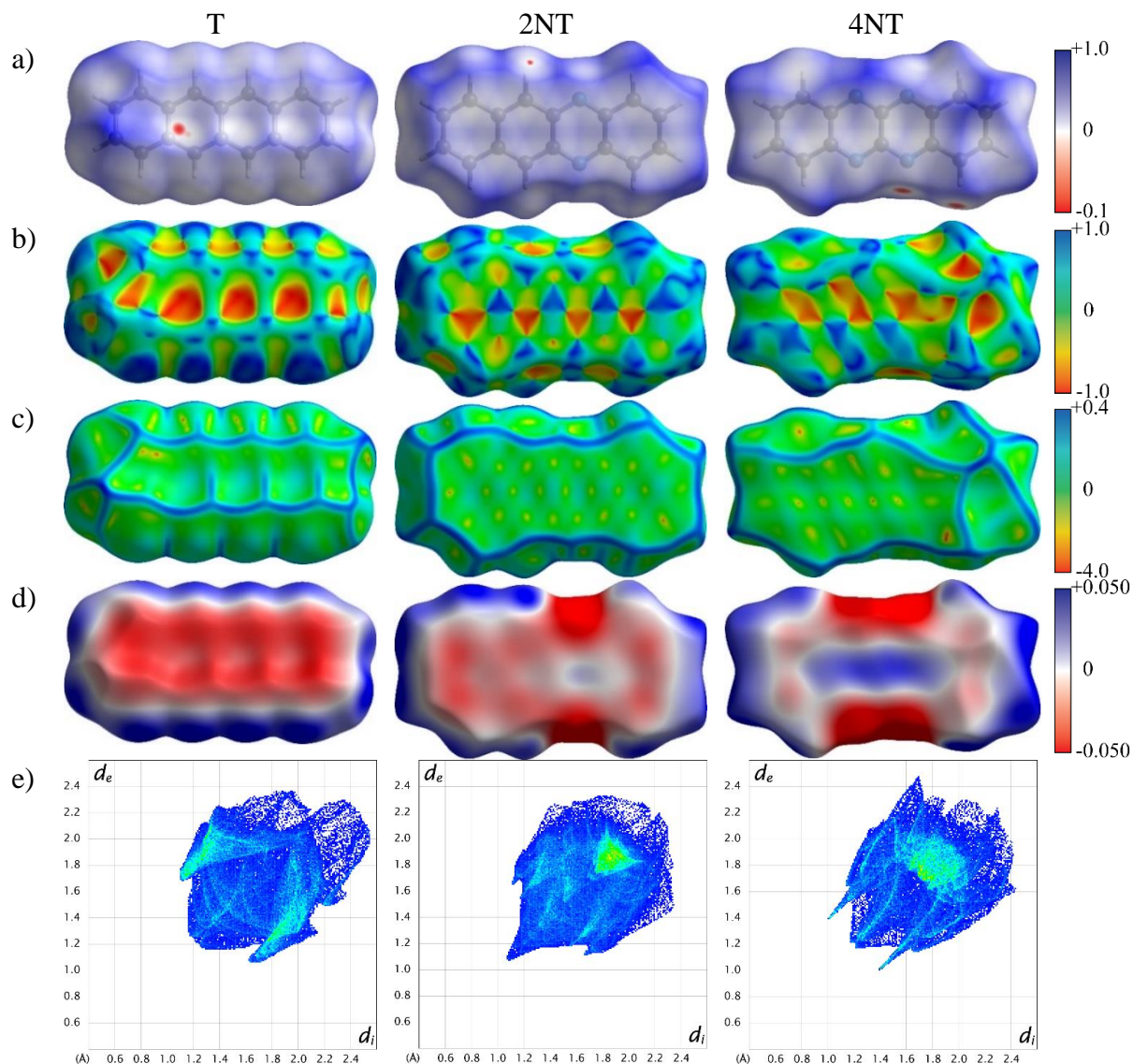


Figure S6. Hirshfeld surfaces for **T**, **2NT** and **4NT** mapped with normalized contact distance (a), shape index (b), curvedness (c) and ESP ( $\pm 65.6 \text{ kJ mol}^{-1}$  per unit charge) (d). Red spots in (a) indicate intermolecular contacts closer than the sum of the van-der-Waals radii (close contacts), blue spots are referred to longer contacts, and contacts around the sum of van-der-Waals radii (moderate contacts) are white. 2D finger print plots (e) with  $d_i$  and  $d_e$  ranging from 0.5 to 2.9 Å. For any given  $d_i$  and  $d_e$  pairs, the change in color shows the raise in occurrence: white color for no occurrence, then blue green and red for the most frequent occurrence.

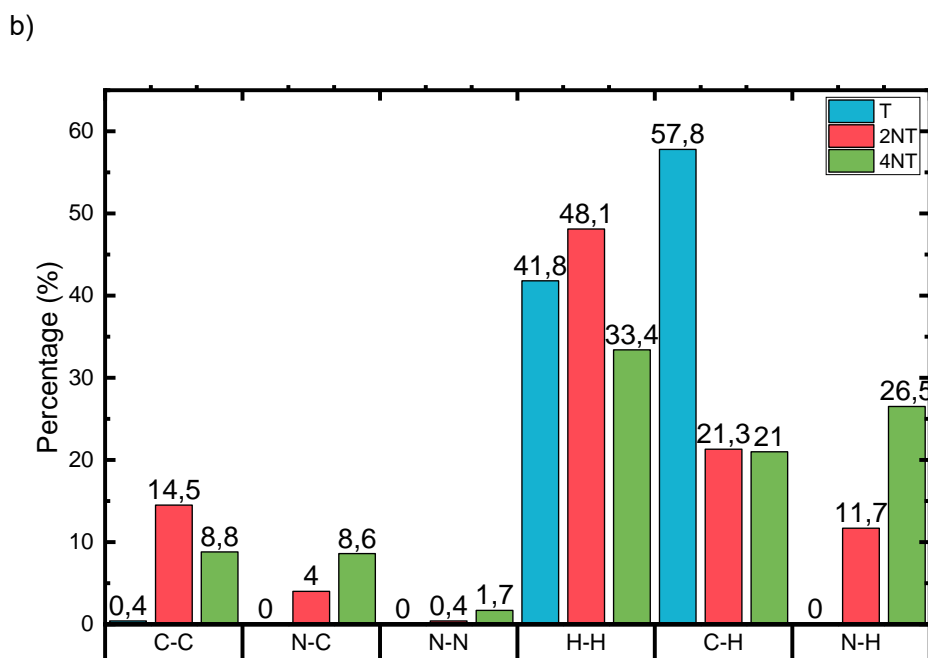
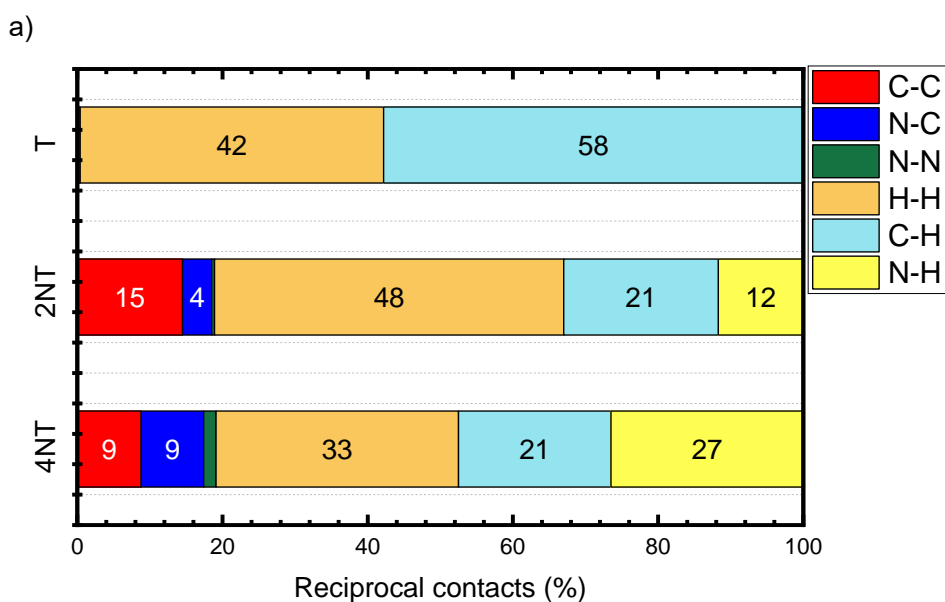


Figure S7. Distribution of reciprocal intermolecular contacts for T, 2NT and 4NT arranged by molecules (a) and atom types (b).

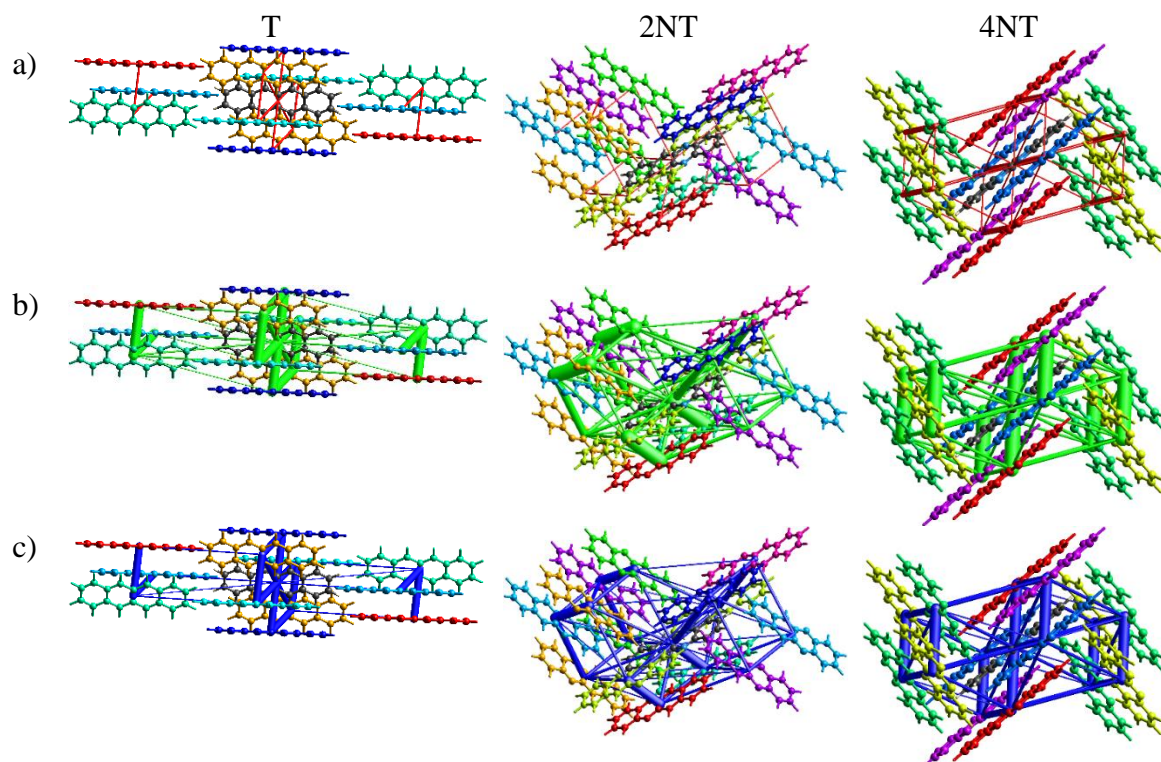


Figure S8. Graphical representation of intermolecular interactions (the Coulomb interaction energy in red on the panel a, the dispersion energy in green on the panel b, and the total interaction energy in blue on the panel c) in **T** (the first column), **2NT** (the second column) and **4NT** (the third column) crystals. The cylinders link molecular centroids, and their thickness is proportional to the magnitude of the energy; for clarity, pairwise energies with magnitudes less than  $5 \text{ kJ mol}^{-1}$  are omitted.

Pentacene and derivatives

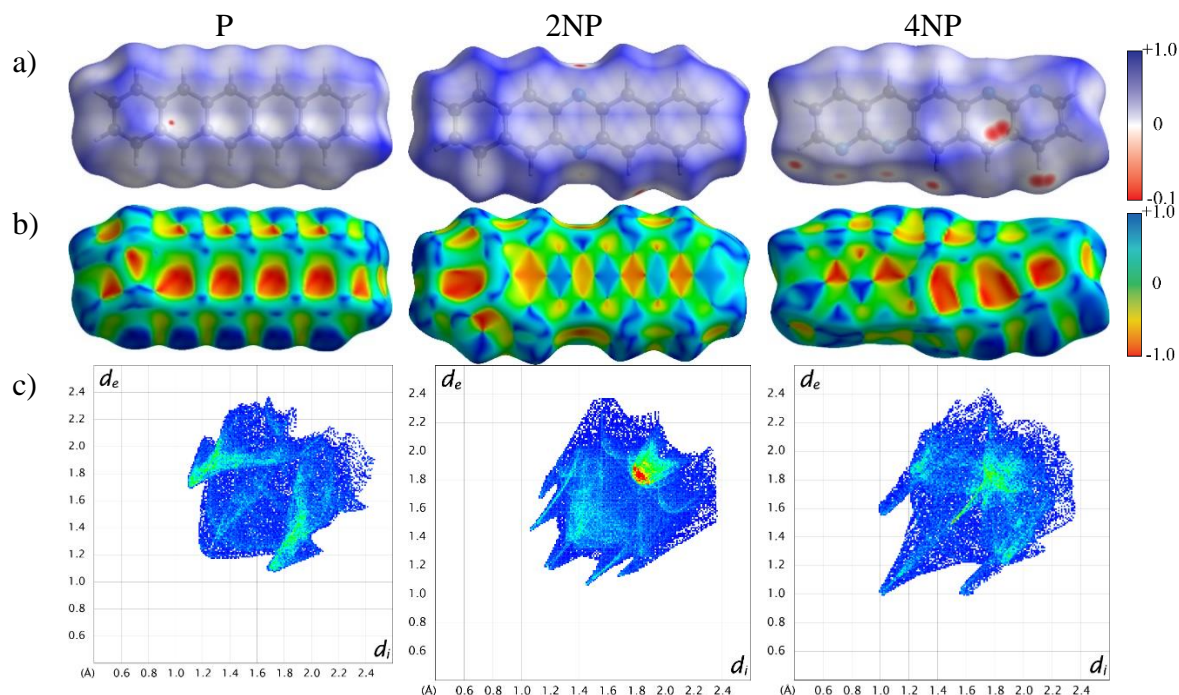


Figure S9. Hirshfeld surfaces for **P**, **2NP** and **4NP** mapped with normalized contact distance (a) and shape index (b). Red spots in (a) indicate intermolecular contacts closer than the sum of the van-der-Waals radii (close contacts), blue spots are referred to longer contacts, and contacts around the sum of van-der-Waals radii (moderate contacts) are white. 2D fingerprint plots (c) with  $d_i$  and  $d_e$  ranging from 0.5 to 2.9 Å. For any given  $d_i$  and  $d_e$  pairs, the change in color shows the raise in occurrence: white color for no occurrence, then blue green and red for the most frequent occurrence.

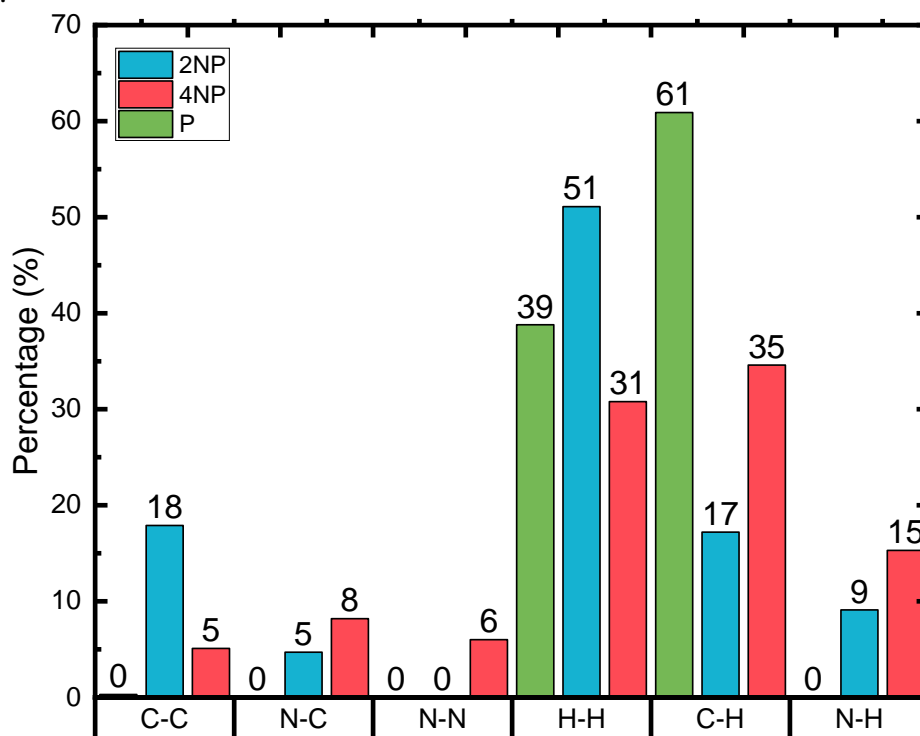


Figure S10. Distribution of reciprocal intermolecular contacts for **P**, **2NP** and **4NP** arranged by atom types.

**P**

**2NP**

**4NP**

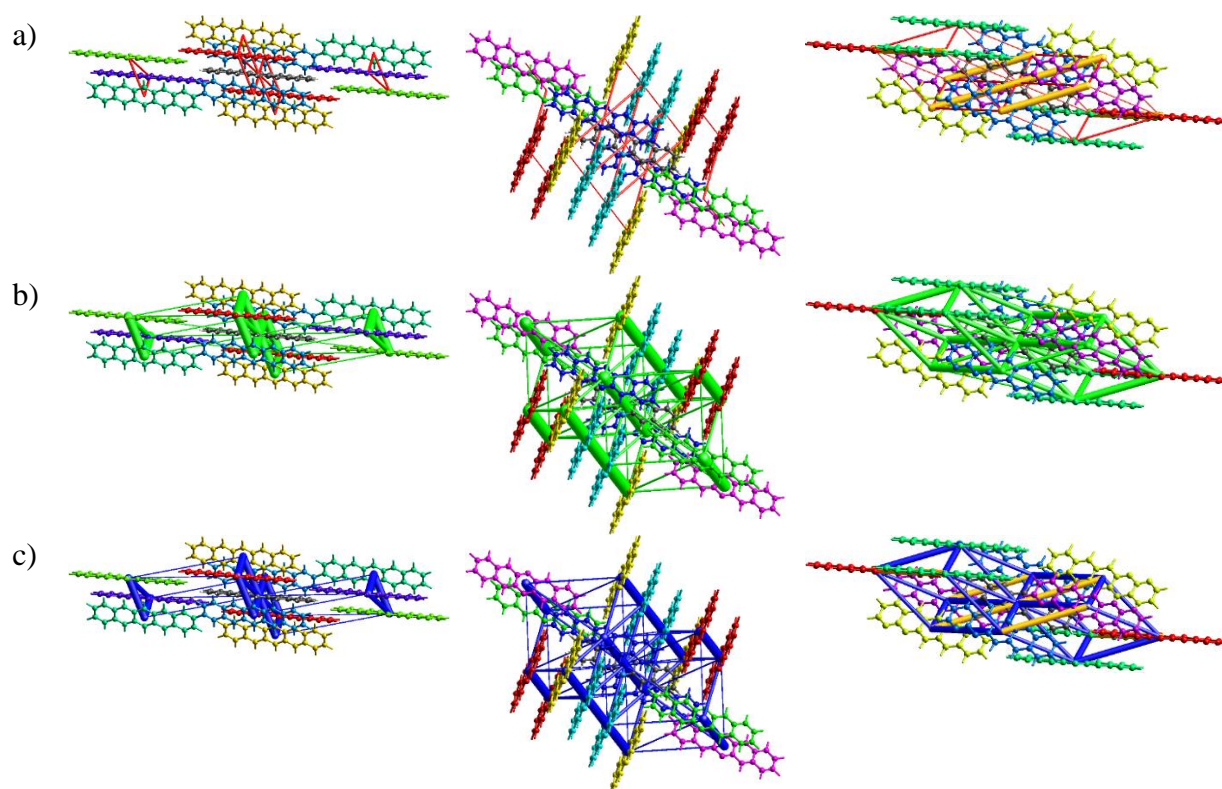
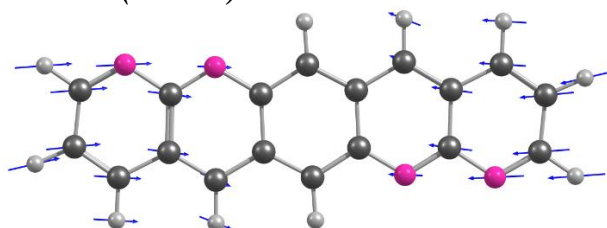


Figure S11. Graphical representation of intermolecular interactions (the Coulomb interaction energy: attraction in red and repulsion in yellow on the panel a, the dispersion energy in green on the panel b, and the total interaction energy in blue on the panel c) in **P** (the first column), **2NP** (the second column) and **4NP** (the third column) crystals. The cylinders link molecular centroids, and their thickness is proportional to the magnitude of the energy; for clarity, pairwise energies with magnitudes less than  $5 \text{ kJ mol}^{-1}$  are omitted.

### S3. Vibrations

$272 \text{ cm}^{-1}$  (mode 1)



$1377 \text{ cm}^{-1}$  (mode 2)

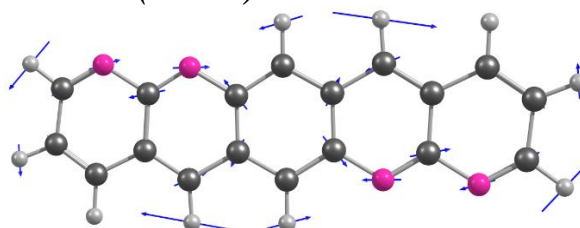


Figure S12. Vibrational displacements for the selected modes of 4NP.

#### S4. Charge mobility details

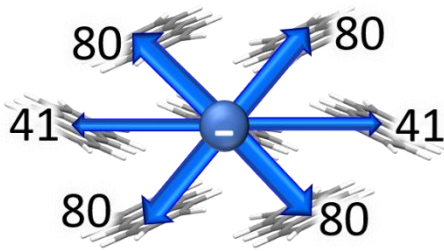
The charge-carrier diffusion coefficient was calculated by summation of the charge transfer rates  $k_i$  determined by Eq. (1) over all the transport directions, i.e. all the pairs of the given molecule with its neighbors:

$$D = \frac{1}{6} \sum_i k_i r_i^2 p_i, \quad (\text{S1})$$

where  $r_i$  is the distance between the molecular centers along the  $i$ -th transport direction, and  $p_i = k_i / \sum_j k_j$  is the probability for the charge to move in this direction. Finally, (isotropic) charge-carrier mobility was estimated using the Einstein–Smoluchowski relation:

$$\mu = \frac{eD}{kT} = \frac{e}{6kT} \sum_i k_i r_i^2 p_i. \quad (\text{S2})$$

a) anthracene



b) tetraazaanthracene

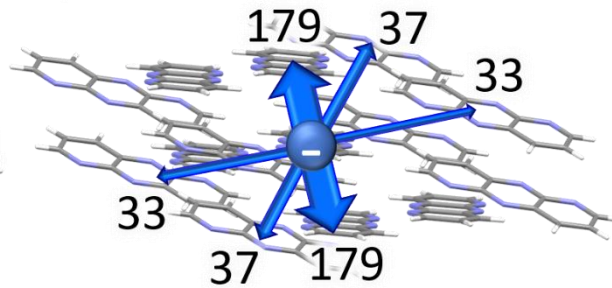


Fig. S13. Electron transfer integrals for **A** and **4NA**.

Table S2. Charge transfer integrals for uracil (left) and adenine (right) crystals.

*Uracil*

*Adenine*

Dimer	$r$ , Å	$J_h$ , meV	$J_e$ , meV
1	3.67	97	47
2	3.67	90	29
3	7.57	-1	1
4	6.27	-29	5
5	6.95	12	-12
6	7.57	-1	1
7	6.27	-31	6
8	6.95	13	-12
9	5.59	-4	25
10	5.99	5	-35
11	8.22	0	0
12	7.37	-1	1
13	6.37	31	-26
14	6.15	15	27
15	6.85	-5	-6
16	6.85	-5	-6
17	6.15	18	29

Dimer	$r$ , Å	$J_h$ , meV	$J_e$ , meV
1	6.50	-11	-23
2	8.50	1	-1
3	8.50	1	-1
4	7.34	8	-46
5	3.79	-61	-22
6	3.79	-59	-20
7	7.34	8	-44
8	6.45	-8	-28
9	10.14	0	0
10	6.32	15	31
11	8.87	0	-0
12	6.78	0	-13
13	6.95	44	-15
14	8.84	0	-1
15	6.69	26	-53
16	6.79	49	-11
17	8.83	0	0